ORIGINAL ARTICLE

# Assessment of a novel *NRAS* in-frame tandem duplication causing a myelodysplastic/myeloproliferative neoplasm

Cora C.A. Beckmann[a], Senthilkumar Ramamoorthy[a,b], Eirini Trompouki[c,d], Wolfgang Driever[e], Stephan Schwarz-Furlan[f], Brigitte Strahm[a], Ayami Yoshimi[a], Charlotte M. Niemeyer[a], Miriam Erlacher[a], and Friedrich G. Kapp[a]*

[a]*Division of Pediatric Hematology and Oncology, Department of Pediatrics and Adolescent Medicine, Faculty of Medicine, University of Freiburg, Freiburg, Germany;* [b]*Institute of Medical Bioinformatics and Systems Medicine, Medical Center, Faculty of Medicine, University of Freiburg, Freiburg, Germany;* [c]*Department of Cellular and Molecular Immunology, Max Planck Institute of Immunobiology and Epigenetics, Freiburg, Germany;* [d]*Institute for Research on Cancer and Aging, Institut National de la Santé et de la Recherche Médicale Unité 1081, Centre National de la Recherche Scientifique, Unité Mixte de Recherche 7284, Université Côte d'Azur, Nice, France;* [e]*Developmental Biology, Faculty of Biology, Institute of Biology 1, Albert-Ludwigs University of Freiburg, Freiburg, Germany;* [f]*Institute of Pathology, Klinikum Kaufbeuren-Ravensburg, Kaufbeuren, Germany.*

Myelodysplastic/myeloproliferative diseases of childhood cause a relevant disease burden, and many of these diseases may have a fatal course. The use of next-generation sequencing (NGS) has led to the identification of novel genetic variants in patients with these diseases, advancing our understanding of the underlying pathophysiology. However, novel mutations can often only be interpreted as variants of unknown significance (VUS), hindering adequate diagnosis and the use of a targeted therapy. To improve variant interpretation and test targeted therapies in a preclinical setting, we are using a rapid zebrafish embryo model that allows functional evaluation of the novel variant and possible therapeutic approaches within days. Thereby, we accelerate the translation from genetic findings to treatment options. Here, we establish this workflow on a novel in-frame tandem duplication in *NRAS* (c.192_227dup; p.G75_E76insDS65_G75) identified by Sanger sequencing in a 2.5-year-old patient with an unclassifiable myelodysplastic/myeloproliferative neoplasm (MDS/MPN-U). We show that this variant results in a myeloproliferative phenotype in zebrafish embryos with expansion of immature myeloid cells in the caudal hematopoietic tissue, which can be reversed by MEK inhibition. Thus, we could reclassify the variant from likely pathogenic to pathogenic using the American College of Medical Genetics (ACMG) criteria. 

## HIGHLIGHTS

- A novel *NRAS* in-frame tandem duplication was found in a patient with unclassifiable MDS/MPN.
- The novel *NRAS* variant results in a myeloproliferative phenotype in zebrafish embryos.
- The novel *NRAS* variant was reclassified from likely pathogenic to pathogenic.
- Therapeutic MEK inhibition reversed myeloproliferation in the animal model.
- The accelerated zebrafish model improves rapid translation from genetics to treatment.

Myelodysplastic and myeloproliferative neoplasms (MDS/MPNs) are a group of heterogeneous clonal hematological diseases with overlapping clinical, genetic, and morphological myelodysplastic and myeloproliferative features [1–3]. MDS/MPNs of childhood are rare with juvenile myelomonocytic leukemia (JMML) being best described [1,4]. Clinical signs of JMML include hepatosplenomegaly and infiltrations of the skin, gut, and lung [4]. Peripheral blood shows leukocytosis with monocytosis and myeloid precursors, thrombocytopenia, and anemia [5]. JMML is caused by mutations resulting in an activated RAS signaling pathway in 90% of the patients. Although mutations in *KRAS, NRAS,* and *PTPN11* are typically acquired somatically, JMML can also arise in the context of predisposition syndromes like neurofibromatosis type I and the Casitas B–lineage lymphoma (CBL) syndrome caused by monoallelic germline *NF1* and *CBL*

Address correspondence to Friedrich G. Kapp, Division of Pediatric Hematology and Oncology, Department of Pediatrics and Adolescent Medicine, Faculty of Medicine, University of Freiburg, Mathildenstr. 1, 79106 Freiburg, Germany; E-mail: friedrich.kapp@uniklinik-freiburg.de

0301-472X/

https://doi.org/10.1016/j.exphem.2024.104207

mutations, respectively [5]. *NRAS* mutations make up to 14%−17% in JMML patients. Amino acid substitutions at positions Gly12, Gly13, or Gln61 lock the NRAS protein in the active guanosine triphosphate-bound state or cause resistance to guanosine triphosphatase (GTPase) activating proteins (GAPs) [5]. Other forms of childhood MDS/MPNs are even rarer, with a more diverse genetic background. Genetic predispositions, such as GATA2 deficiency and RUNX1 deficiency, present mainly with myelodysplastic syndrome (MDS) but can also present as an MDS/MPN overlap syndrome [6]. Broad next-generation sequencing analyses (including gene panels, whole exome sequencing (WES), and even whole genome sequencing) may result in the identification of novel variants, which often are of unknown significance (VUS). To accelerate finding of the correct diagnosis and pave the way for targeted therapies, we established an in vivo zebrafish-based assay that allows for rapid functional assessment of novel variants and facilitates the selection of treatment targets. The zebrafish is a promising model system to study the human hematopoietic system because many signaling pathways in hematopoietic development were shown to be conserved. In addition, humans and zebrafish share all major blood cell types, and hematopoietic stem and progenitor cells (HSPCs) are regulated by similar cues [7]. Moreover, genetic manipulation of the zebrafish embryo is achieved easily [7]. Here, we use these advantages to study the effect of a novel *NRAS* in-frame tandem duplication (c.192_227dup; p.G75_E76insDS65_G75) (referred to as $NRAS^{ITD}$, hereafter) identified in a young patient with unclassifiable MDS/MPN (MDS/MPN-U). Tissue-specific overexpression of this novel variant in endothelial and hematopoietic cells of zebrafish embryos leads to a myeloproliferative phenotype in the zebrafish that can be prevented by treatment with the MEK inhibitors PD0325901 and trametinib, corroborating the causative nature of this novel mutation.

## METHODS

### Wild-Type and Transgenic Zebrafish Lines

Zebrafish (*Danio rerio*) was used as animal model. The transgenic zebrafish line *Tg(fli1a:Gal4)* (officially $Tg(fli1a:Gal4FF)^{ubs3}$) was kindly provided by the Affolter lab at the Biozentrum Basel, Switzerland [8]. *Tg(runx:Gal4)*, or officially $Tg(Mmu.runx1:GAL4)^{utm6}$, containing the Gal4 gene under the control of the regulatory mouse Runx 1 + 23 enhancer elements and a mouse $\beta$-globin minimal promotor was created and kindly provided by Marina Mione from the Centre for Integrative Biology, University of Trento, Italy. All experiments were performed in accordance with relevant guidelines and regulations of the University Freiburg and the Regierungspräsidium Freiburg. Zebrafish husbandry was conducted according to standard protocols [9].

### Cloning of UAS:NRAS Constructs

The sequence of the gene *NRAS* (c.192_227dup; p.G75_E76insDS65_G75) (abbreviated as $NRAS^{G75\_E76insDS65\_G75}$ or $NRAS^{ITD}$) was codon optimized for zebrafish codons using the codon optimization tool from Integrated DNA Technologies (IDT, https://www.idtdna.com/codonopt) as it was reported that codon optimization increases expression in zebrafish [10]. The optimized sequence was ordered as chemically synthesized, double-stranded gene fragments, commercially available as gBlocks (IDT). The *NRAS* gene was designed without a stop codon followed by a P2A-green fluorescent protein (GFP) tag.

To integrate the gBlock into a pME plasmid, a KpnI restriction site was inserted into the pME-Cherry plasmid using the Q5 Site-Directed Mutagenesis Kit (New England Biolabs [NEB], E0554S). Mutagenesis primers were designed using the NEBaseChanger tool (NEB, forward primer: CTCGAGCACCCAGCTTTCTTGTAC, reverse primer: GGTACCTTACTTGTACAGCTCGTC). All plasmids were validated by sequencing.

Next, 5 $\mu$g modified pME-mCherry plasmid DNA was double digested with KpnI (Thermo Fisher, ER0521) and NcoI (Thermo Fisher, ER0571) restriction enzymes for 1 hour at 37°C to remove the mCherry sequence, followed by gel purification of the plasmid backbone using the Wizard SV Gel and polymerase chain reaction (PCR) Clean-Up System (Promega, A9281) following the manufacturer's protocol. The gBlock $NRAS^{G75\_E76insDS65\_G75}$ (IDT) was fused with the linearized and purified plasmid backbone using the Gibson Assembly cloning kit (NEB, E5510S) following the manufacturer's protocol [11]. Successful assembly was checked by restriction digest and sequencing.

The pME-$NRAS^{ITD}$ plasmid was then modified to pME-$NRAS^{wt}$ using the Q5 Site-Directed Mutagenesis Kit (NEB, E0554S) and mutagenesis primers (forward primer: AGCGCCATGAGAGACCAG, reverse primer: GTACTCCTCCTGTCCGGC).

### Gateway™ Cloning

Following the protocol for the Gateway™ LR Clonase™ II Plus (Thermo Fisher, 12538120), we combined four plasmids: the middle entry clone (pME, e.g. pME:$NRAS^{ITD}$), the 5'-entry clone (e.g., p5E:UAS, containing the upstream activating sequence (UAS)), the 3'-entry clone (e.g., p3E-P2A-GFP) and the destination vector (e.g. pDEST:Tol2pA2) (Table 1). Changes to the protocol included a prolongation of the incubation step up to 24 hours at room temperature. The success of recombination was verified by a restriction digest.

### Preparation of Tol2 Transposase for Mosaic Expression of UAS: NRAS Constructs

Capped messenger RNA (mRNA) encoding the Tol2 transposase was transcribed in vitro using pCS2FA-transposase as a template (Tol2Kit [396], Kristen Kwan, Chien lab). After linearization with NotI (NEB, R0189S), in vitro transcription of mRNA using the mMessage mMachine SP6 transcription kit (Thermo Fisher, AM1340) was performed. The transposase facilitates the integration of the Tol2-flanked sequence into the zebrafish's genome [12]. To achieve a mosaic, tissue-specific expression, the UAS—"gene-of-interest"—construct was injected into *Tg(fli1a:Gal4)* to limit the expression to endothelial and early HSPCs [13] and into *Tg(runx:Gal4)* for expression in HSPCs only [14].

**Table 1** Plasmids recombined by gateway cloning

| Final Plasmid | Cloned from plasmids |
|---|---|
| UAS:$NRAS^{wt}$ | pME:$NRAS^{wt}$, p5E:UAS, p3E-P2A-GFP, pDEST:Tol2pA2 |
| UAS:$NRAS^{ITD}$ | pME:$NRAS^{ITD}$, p5E:UAS, p3E-P2A-GFP, pDEST:Tol2pA2 |

GFP=Green fluorescent protein; ITD=internal tandem duplication; p5E, pME, p3E, pDEST=5' entry, middle entry, 3' entry and destination vectors for Gateway cloning, respectively; UAS=upstream activating sequence;wt=wild type

### Plasmid Injection

Approximately 25 pg of plasmid with 12 pg of Tol2 transposase mRNA (approximately 1 nL of an injection mix with the concentration of 50 ng/$\mu$L of plasmid and 45 ng/$\mu$L of Tol2 mRNA) were injected into zebrafish embryos at the single-cell stage using thin-wall glass capillaries (World Precision Instruments, TW100F-4) and the Pneumatic Pico Pump 820 (World Precision Instruments, SYS-PV820).

For better readability, *Tg(fli1a:Gal4FF$^{\mu bs3}$; UAS:RFP)* embryos injected with the gene of interest (e.g., UAS:*NRAS$^{ITD}$*-P2A-*GFP*) and Tol2 mRNA are abbreviated as *fli1a:NRAS$^{ITD}$*$_{G0mosaic}$ instead of *Tg(fli1a:Gal4FF$^{\mu bs3}$; UAS:RFP)*, *Tg(UAS:NRAS$^{ITD}$*-P2A-*GFP)*$_{G0\ mosaic}$.

### Pharmacological Treatment

The zebrafish embryos were randomized into control and treatment groups and incubated from 12 hours post fertilization (hpf) with different chemicals until 48 or 72 hpf. The chemicals were diluted to the intended concentration in E3 medium: lipopolysaccharide (LPS) 100 $\mu$g/mL (Sigma-Aldrich, L2630), methotrexate (MTX) 500 $\mu$M (Sigma-Aldrich, A6770), peroxisome-proliferator activated receptor $\delta$ (PPAR$\delta$) antagonist GSK3787 500 nM (BioVision, ref 2400), PD0325901 0.5 $\mu$M (Cayman Chemical, 13034), and trametinib 50 nM (Cayman Chemical, 16292).

### Peripheral Blood Cell and Caudal Hematopoietic Tissue Smears

The expression of the injected plasmid was controlled by examination of the reporter gene activity using a fluorescence stereomicroscope. Embryos were selected that showed a similar transgene integration efficiency as judged by the presence of GFP in blood and endothelial cells (coexpressed with the gene of interest based on the P2A linker).

Forty-eight hpf to 5 days post fertilization (dpf) zebrafish were kept in a petri dish in an optimized solution containing 0.9% sodium chloride (NaCl) with 5% fetal bovine serum (FBS) and 0.168 mg/mL tricaine. Zebrafish peripheral blood cells (PBCs) and caudal hematopoietic tissue (CHT) were collected by cutting the zebrafish embryo's tail just distal to the cloaca and end of the yolk sac extension.

For tissue digestion, the tail was incubated with 5 mg/mL of Liberase (Roche, 05401119001) at a dilution of 1:64 for 20 minutes at 37° C. FBS was added to a final concentration of 10 % to stop the digestion process. For further separation of the tissue the suspension was triturated and passed through a 40-$\mu$m cell strainer to remove debris. Cytospins were prepared from PBCs and CHT suspension by centrifugation with 800 rounds per minute (rpm) for 10 minutes followed by May-Grünwald Giemsa (MGG) staining. Analysis was performed using the Nikon Eclipse 80i microscope.

### Image Analysis

The analysis of erythrocyte cell size and chromaticity was performed using FIJI / ImageJ. Images were converted to 8-bit files [15]. The nucleus was captured using the threshold "minimum," whereas the cytoplasm was measured using the threshold "triangle".

### Statistical Analysis

Analysis and statistics were performed using Prism GraphPad Software 7.01, the $X^2$ test calculator from Social Science Statistics (Jeremy Stangroom, socialsciencestatistics.com) and Microsoft Office Excel 2008.

Differences in the cell populations in the CHT between control and mutant embryos were analyzed using the $X^2$ test. For the analysis of erythrocyte morphology in zebrafish embryos treated with chemicals, the unpaired *t* test was used.

The probability value was Bonferroni corrected and considered significant when $p \leq \frac{\alpha}{m}$, with $\alpha = 0.05$ and m is the number of hypotheses.

Experiments were conducted in a blinded fashion, whenever possible. Animals were randomly assigned to treatment and control groups.

## RESULTS

### Novel NRAS$^{ITD}$ Identified in a Patient With an MDS/MPN

A 2.5 year-old girl presented with a massive hepatosplenomegaly that resulted in tachypnea (Figure 1A). Anemia (6.6 G/dL hemoglobin) as well as thrombocytopenia (67 G/L platelets) were found, whereas leukocyte and neutrophil counts (4.6 G/L and 1.6 G/L, respectively) were normal. Peripheral blood smears showed myeloid and erythroid precursors and a few myeloblasts (<1%) but no monocytosis. Dacrocytes were present as a possible sign of myelofibrosis (Figure 1B). The bone marrow smear was not fully representative due to the presence of myelofibrosis, but a left-shifted myelopoiesis with disturbed maturation and mild dysplasia were observed, as well as erythropoiesis with moderate dysplastic features, such as double nuclei and cytoplasmic bridges. There was no excess of blasts. The trephine biopsy (Figure 1C and 1D) showed hypercellular bone marrow with slight to moderate myelofibrosis (MF; MF1, focally MF2 according to World Health Organization [WHO] classification), hyperplasia of a left-shifted myelopoiesis, hypoplasia of erythropoiesis, a slightly increased number of megakaryocytes, and infiltration of B lymphocytes. Given the JMML-like presentation with massive hepatosplenomegaly, myeloid and erythroid precursors in peripheral blood, anemia, and thrombocytopenia, JMML-associated genes were analyzed by Sanger sequencing of the patient's bone marrow. A somatic *NRAS* variant (c.192_227dup; p.G75_E76insDS65_G75) (*NRAS$^{ITD}$*), leading to a duplication of 11 amino acids in the *NRAS* Switch II motif/region was found (Figure 1E) [16–18]. Based on American College of Medical Genetics (ACMG) criteria, the variant was interpreted as likely pathogenic (Criteria for Classifying Pathogenic Variants: PM1 + PM2 + PM4 + PP3). It was not present in gnomAD (v3.1.2) or COSMIC (COSMICdb, v98, Wellcome Sanger Institute) [19].

The majority of the oncogenic *NRAS* mutations are missense at codons G12, G13, and Q61, whereas in-frame insertions account for less than 0.1% of the described mutations and are located in exons 2 and 3 (COSMICdb, v98) [20]. The *NRAS$^{ITD}$* mutation was absent in hair follicles of the patient and the parents' blood. Because of the unclear contribution of the NRAS variant to the disease, WES was performed but no other disease-causing mutations were found in both the patient and her parents (Supplementary Table E1). *NRAS$^{ITD}$* was found with a variant allele frequency (VAF) of 22% (39/177 total reads) of the WES data in the bone marrow of the child.

Due to the severity of the disease, hematopoietic stem cell transplantation (HSCT) was considered the only curative treatment. After a myeloablative conditioning regimen with busulfan, cyclophosphamide, melphalan, and antithymocyte globulin, the patient received a bone marrow transplant from a human leukocyte antigen (HLA)-identical unrelated donor. The graft contained $8.79 \times 10^8$ nucleated cells/kg body weight, corresponding to $9.05 \times 10^6$ CD34-positive

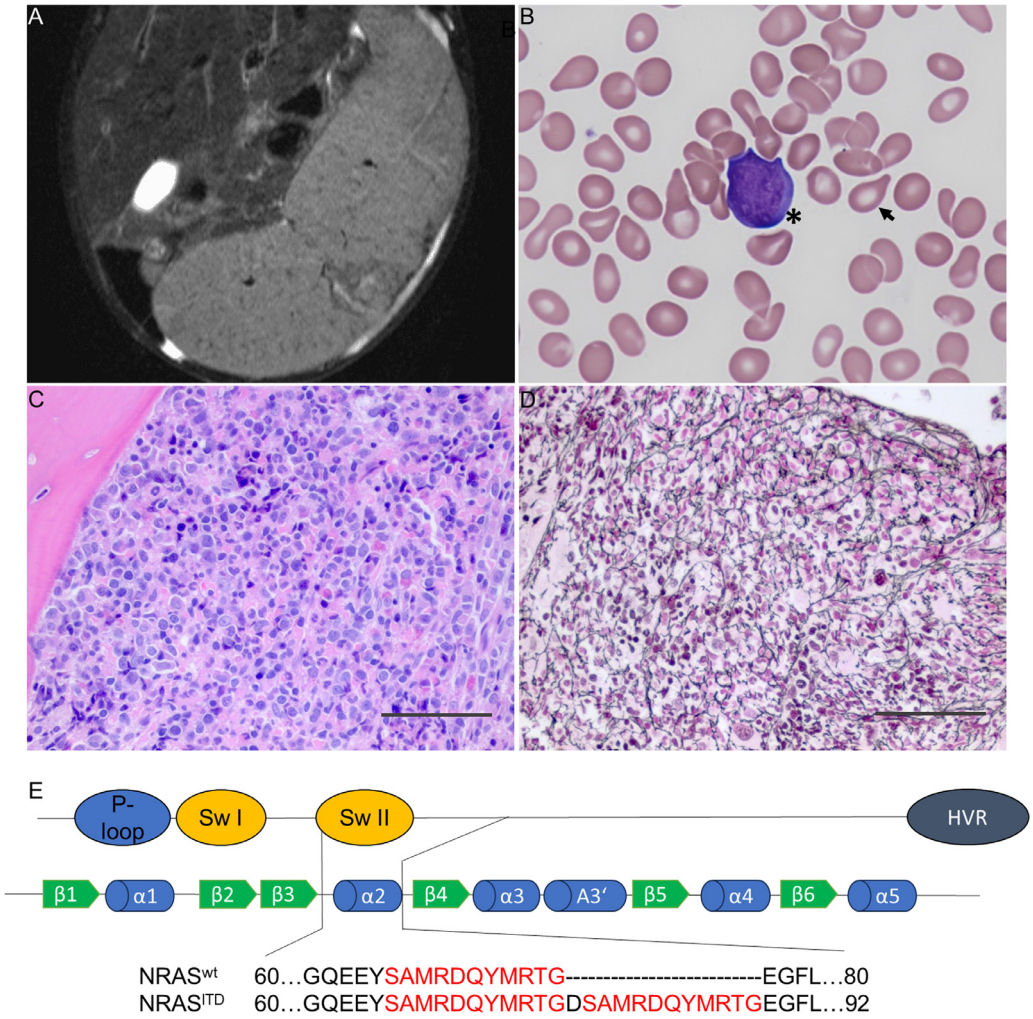


Figure 1 Phenotype of the affected child and the novel NRAS$^{ITD}$ mutation. **(A)** The 2.5-year-old child suffered from a severe hepatomegaly and especially splenomegaly as shown in the magnetic resonance image (T2 sequence with fat saturation). **(B)** In peripheral blood smears taken at first presentation to our clinic, blast cells (asterisk) were found as well as dacrocytes (arrow) as a sign of myelofibrosis. **(C)** The trephine biopsy specimen obtained showed hypercellular bone marrow (hematoxylin and eosin stain, 400 ×) with hyperplasia of a left-shifted granulopoiesis, hypoplasia of the erythropoiesis (scale bar: 50 μm), and **(D)** myelofibrosis (Gomori's silver staining, 400 ×, scale bar: 50 μm). **(E)** In the patient's bone marrow, the somatic NRAS$^{ITD}$ mutation was found by Sanger sequencing, leading to a duplication of 11 amino acids. Shown is an alignment to the GTPase NRAS *Homo sapiens* Sequence ID: NP 002515.1 using BLASTp (NCBI) [17,18]. The location of the duplication in correlation to the P-loop, switch I (Sw I) and switch II (Sw II) domains, and the hypervariable region (HVR) of the NRAS protein is shown. Underneath, the secondary structural elements of the NRAS protein are shown as green arrows and blue cylinders representing β-sheets and α-helices, respectively [16].

cells/kg body weight. Graft-versus-host disease prophylaxis was performed with cyclosporin A.

On day 5 after stem cell infusion, the patient developed increasing tachydyspnea and was transferred to the intensive care unit. After initial stabilization with respiratory support via high-flow nasal cannula, she had to be intubated due to respiratory muscle fatigue leading to respiratory failure on day 8 after HSCT. High ventilator pressures were immediately necessary, and she eventually developed pulmonary hemorrhage in the setting of disseminated intravascular coagulation, precluding adequate oxygenation and ventilation. Additionally, circulatory failure requiring catecholamine support occurred on day 8 after HSCT; normotension could not be achieved despite vasopressor treatment with dopamine, epinephrine, norepinephrine, and milrinone. Multiple organ dysfunction progressed with anuria and renal insufficiency requiring dialysis on day 9. Additionally, liver failure progressed without signs of a veno-occlusive disease, and the patient passed away 10 days after HSCT.

## Establishment of the Model System

Due to the severity of the disease and its unusual clinical presentation, we set out to model the novel variant using zebrafish embryos. As a first step to establish this model, we assessed zebrafish blood cell morphology in wild-type (WT) zebrafish embryos after treatment with

MTX and LPS and could observe anticipated changes in hematopoiesis, namely macrocytic and hyperchromic erythrocytes in the peripheral blood of MTX-treated embryos and an increased fraction of mature myeloid cells in the CHT of LPS-treated embryos (Supplementary Figure E1).

As establishing stable transgenic lines is a time-consuming process, hindering its use in a clinical setting, we tested the accelerated assessment of a genetic variant by analysis of plasmid-injected embryos next. To this end, we injected the plasmid containing the genetic variant of interest into *Tg(fli1a:Gal4)* embryos. In these embryos, the fli1a promoter drives Gal4 expression in cells of the lateral plate mesoderm that give rise to endothelial and hematopoietic cells [13]. Thus, Gal4 expression is restricted to vascular and hematopoietic cells and in turn activates the UAS element contained in the injected plasmid that randomly integrates into the cells of the zebrafish in a tissue-specific manner and thus restricts expression of the gene of interest. To facilitate integration of the injected plasmid into the genome, Tol2 transposase mRNA was injected together with the plasmid (Supplementary Figure E2A).

Before analysis of the novel $NRAS^{ITD}$ variant, we tested the model system using the human acute myeloid leukemia (AML)−causing gene H2.0-like homeobox (*HLX*). As was shown previously, stable overexpression of *HLX* in endothelial and hematopoietic cells by crossing a *Tg(fli1a:Gal4)* or *Tg(runx1+23:Gal4)* fish to *Tg(UAS:HLX)* fish leads to an increase in the immature myeloid cell fraction [21] comparable to the block in myeloid differentiation observed in human AML [22]. The HLX effect on zebrafish blood cell morphology could be abrogated by inhibition of the PPARδ pathway downstream of HLX [21]. Indeed, the mosaic overexpression of *HLX* led to an increased fraction of immature myeloid cells in $fli1a{:}HLX_{G0mosaic}$ embryos at 48 hpf (Supplementary Figure E2B and E2C), similar to what was known from stable overexpression, confirming the reliability of the mosaic overexpression system. By inhibition of the PPARδ pathway in $fli1a{:}HLX_{G0mosaic}$ embryos using GSK3787 from 12 hpf to 48 hpf (Supplementary Figure E2A), the fraction of immature myeloid cells normalized again (Supplementary Figure E2B and E2C), similar to what could be observed when working with stable transgenic lines.

### $NRAS^{ITD}$ Expression in Zebrafish Embryos Results in Myeloproliferation

At first, the UAS:$NRAS^{ITD}$ plasmid was tested for unspecific side effects by injection into WT zebrafish embryos, where no comparable morphological phenotype could be observed. There was no difference in immature myeloid and mature myeloid cell fractions between WT embryos injected with the UAS:$NRAS^{ITD}$ plasmid and uninjected WT embryos, but less erythroid cells were seen in WT embryos injected with the UAS:$NRAS^{ITD}$ plasmid compared with uninjected WT embryos (Supplementary Figure E3). We then applied the new model system to assess the hematologic phenotype induced by tissue-specific endothelial and hematopoietic overexpression of the $NRAS^{ITD}$ variant identified in our patient in $fli1a{:}NRAS^{ITD}{}_{G0mosaic}$ embryos and compared their blood cell morphology to $fli1a{:}NRAS^{wt}{}_{G0mosaic}$ embryos and uninjected *Tg(fli1a:Gal4)* embryos (Figure 2A). We observed a significant increase in the immature myeloid cell fraction resembling the left-shifted myelopoiesis observed in the child (Figure 2B and 2C). Interestingly, we also observed an increase in immature myeloid cells in $fli1a{:}NRAS^{wt}{}_{G0mosaic}$ embryos compared with uninjected embryos.

To rule out a noncell autonomous effect on hematopoiesis mediated through endothelial cells, the $NRAS^{ITD}$ plasmid was also expressed using the runx1+23 promoter that restricts expression to HSPCs [14]. To this end, we injected the UAS:NRAS constructs into *Tg(runx:Gal4)* embryos. In $runx{:}NRAS^{ITD}{}_{G0mosaic}$ embryos, we observed an increased fraction of immature myeloid cells in the CHT compared with uninjected *Tg(runx:Gal4)* and $runx{:}NRAS^{w}{}_{G0mosaic}$ embryos (Figure 2D and 2E), suggesting a cell-autonomous effect of the $NRAS^{ITD}$ mutation in HSPCs.

To further characterize the novel $NRAS^{ITD}$ variant, the hematologic phenotype of $fli1a{:}NRAS^{ITD}{}_{G0\ mosaic}$ embryos was compared with embryos injected with the constitutive active $NRAS^{G12D}$ and the dominant negative $NRAS^{S17N}$ as well as to $NRAS^{wt}$-expressing *Tg(fli1a:Gal4)* embryos. $fli1a{:}NRAS^{ITD}{}_{G0\ mosaic}$ embryos showed the strongest increase in the immature myeloid cell fraction in the CHT (Supplementary Figure E4). Both $NRAS^{wt}$ and $NRAS^{G12D}$ also led to an increase of immature myeloid cells, whereas the dominant negative $NRAS^{S17N}$ variant did not influence the hematologic phenotype.

We next performed drug treatments to identify chemicals capable of reversing the myeloproliferative phenotype induced by $NRAS^{ITD}$-overexpression (Figure 3A). PD0325901 and trametinib are allosteric MEK inhibitors [23,24], thus inhibiting MEK, the main kinase downstream of NRAS [25]. Beforehand, MEK inhibitor treatment was tested in uninjected *Tg(fli1a:Gal4)* embryos, and a slight decrease in immature myeloid cells, not significant for trametinib but significant for PD0325901, was observed (Supplementary Figure E5). In the embryos injected with the $NRAS^{ITD}$ plasmid, both inhibitors prevented the $NRAS^{ITD}$ phenotype, showing no significant difference compared with uninjected *Tg(fli1a:Gal4)* embryos (Figure 3B and 3C).

## DISCUSSION

Understanding the genetic basis of hematopoietic diseases is crucial for correct diagnosis and identification of novel and targeted treatments. Here, we characterize a novel, likely pathogenic $NRAS^{ITD}$ variant in a patient with a myeloproliferative disorder that was difficult to classify. The extensive splenomegaly and the affected gene were compatible with JMML, but the patient did not exhibit leukocytosis or monocytosis, among other key diagnostic parameters for JMML. Signs of bone marrow dysplasia could be observed, in line with a MDS, but the bone marrow showed an unusual degree of myelofibrosis (MF1, focally MF2 according to the WHO 2018 classification). The clinical picture did not meet the diagnostic criteria for a specific MDS, a specific myeloproliferative neoplasia (MPN) subtype, or a specific MDS/MPN subtype, and in the end, an MDS/MPN-U was diagnosed. MDS/MPN-U is a subgroup of myeloid neoplasms defined by overlapping pathology and molecular features of MDS/MPNs that do not meet the criteria for JMML or atypical chronic myeloid leukemia (aCML) [3]. Earlier in the literature, the hematological disease in a child with a *KRAS* insertion mutation presenting with hepatosplenomegaly, hypercellular bone marrow without myelodysplasia, monocytosis and pancytopenia was described as an atypical or unclassifiable myeloproliferative neoplasm (MPN-U) [26]. Despite related RAS duplication mutations in that patient and in our case, the clinical presentation was different.

Like the disease, the mutation was difficult to interpret. Although ACMG criteria resulted in classification as likely pathogenic variant, the unusual duplication mutation did not correspond to the typical

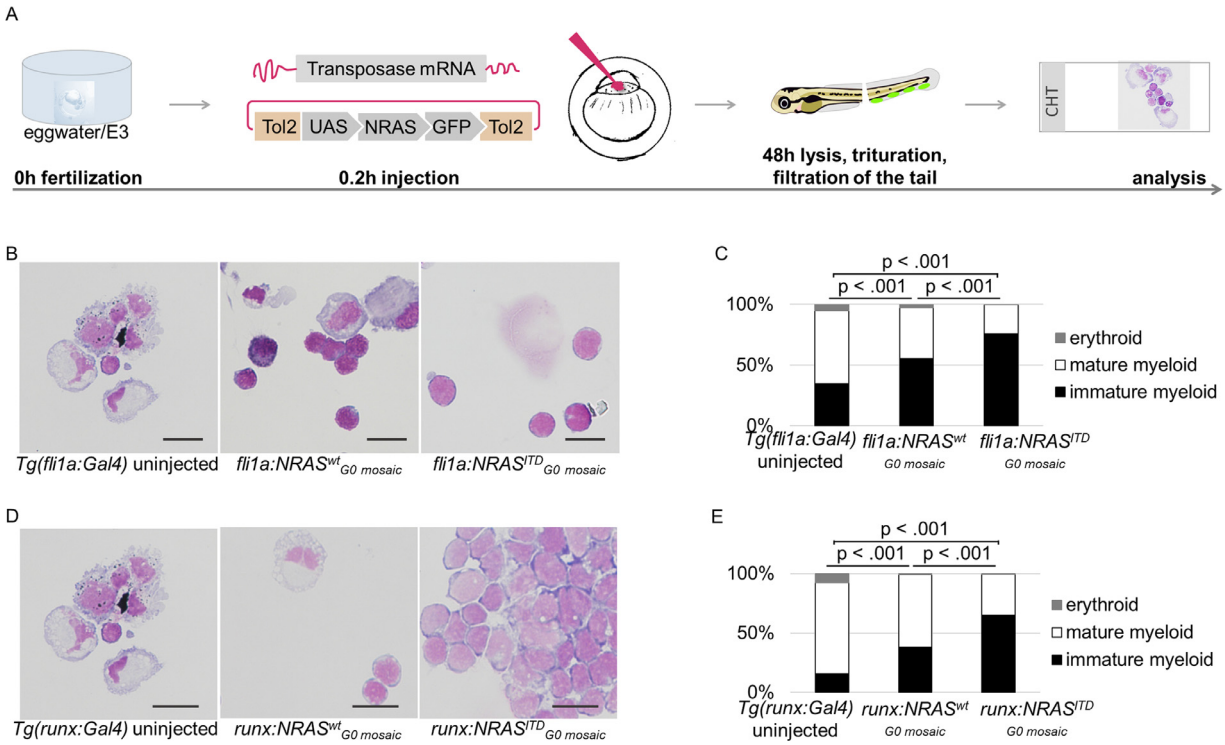


Figure 2 Functional assessment of *NRAS*$^{ITD}$ in zebrafish embryos. **(A)** The NRAS-plasmid was coinjected with Tol2 transposase messenger RNA (mRNA) into the single-cell embryo. Zebrafish embryos' caudal hematopoietic tissues (CHTs) were analyzed at 48 hours post fertilization (hpf). **(B)** Images show CHT smears stained with May-Grünwald Giemsa (MGG) stain in *fli1a:NRAS*$^{ITD}{}_{G0mosaic}$, *fli1a:NRAS*$^{wt}{}_{G0mosaic}$, and uninjected *Tg(fli1a:Gal4)* embryos at 48 hpf. Scale bar: 10 $\mu$m. **(C)** Shown are ratios of cell populations in CHT smears from four embryos per condition as percentages. *fli1a:NRAS*$^{ITD}{}_{G0mosaic}$ embryos showed an increased fraction of immature myeloid cells compared with uninjected *Tg(fli1a:Gal4)* embryos ($X^2$ [2, n=4] = 67.59, $p < 0.001$) as well as to *fli1a:NRAS*$^{wt}{}_{G0mosaic}$ ($X^2$ [2, n=4] = 22.41, $p < 0.001$) at 48 hpf. In addition, in *fli1a:NRAS*$^{wt}{}_{G0mosaic}$ embryos, an immature myeloid expansion was observed compared with uninjected *Tg(fli1a:Gal4)* embryos ($X^2$ [2, n=4] = 15.12, $p < 0.001$). **(D)** Images show CHT smears stained with MGG stain in *runx:NRAS*$^{ITD}{}_{G0mosaic}$, *runx:NRAS*$^{wt}{}_{G0mosaic}$, and uninjected *Tg(runx:Gal4)* embryos at 5 days post fertilization (dpf). Scale bar: 10 $\mu$M. **(E)** Shown are ratios of cell populations in CHT smears from four embryos per condition as percentages. *runx:NRAS*$^{ITD}{}_{G0mosaic}$ embryos showed an increase in the immature myeloid cell fraction compared with uninjected *Tg(runx:Gal4)* embryos ($X^2$ [2, n=4] = 112.04, $p < 0.001$) at 5 dpf. In addition, in *runx:NRAS*$^{wt}{}_{G0mosaic}$ embryos, an immature myeloid expansion was observed compared with uninjected *Tg(runx:Gal4)* embryos ($X^2$ [2, n=4] = 21.53, $p < 0.001$).

JMML-associated point mutations. It seemed that the unclassifiable disease subtype might be compatible with this unusual *NRAS*$^{ITD}$ variant. Pathogenicity of the mutation was suspected because similar RAS indels in the switch II motif have been described among others in colorectal cancer [27], vascular anomalies [28], and an atypical MPN [26]. To further classify this mutation and assess its effect on hematopoiesis, we optimized our zebrafish model to rapidly study both the pathogenicity of the novel variant as well as the response to drug treatments, omitting the time-consuming step of establishing stable transgenic zebrafish lines.

In the chemical treatments, we could monitor expected effects on early hematopoiesis by analyzing blood cell morphology, namely the picture of an activated immune system with an increased fraction of mature myeloid cells in the CHT of LPS-treated embryos and erythrocytes resembling folic acid deficiency anemia in MTX-treated embryos.

To rapidly assess genetic perturbations, we showed that mosaic *HLX* overexpression led to an increased fraction of immature myeloid cells in the CHT of *fli1a:HLX*$_{C0mosaic}$ embryos. Thus, we could replicate the results of stable *HLX* expression [21]. We also show that the mosaic expression system could be used to assess the effect of drug treatment, again replicating the results of drug treatment in stable lines [21].

The novel *NRAS*$^{ITD}$ variant identified in our patient was a somatic variant, making the use of our mosaic expression system reasonable, as it would mimic the situation in the patient. As a limitation, random integration of the plasmid must be mentioned, which on its own may already have effects on hematopoiesis. However, expression of a mutation from the endogenous locus is very difficult to achieve, especially in a mosaic expression system. We tried to control for this effect by analyzing different *NRAS* variants and multiple embryos per experiment to minimize the risk of biased results. In the future, standardized landing sites might be helpful, such as described by Lalonde et al. [29]. In this work, we controlled for the effects of random integration using multiple lines of evidence by comparing two promoters (fli1a and runx1) and multiple *NRAS* variants, including the dominant negative *NRAS*$^{S17N}$, which did not affect the hematological phenotype.

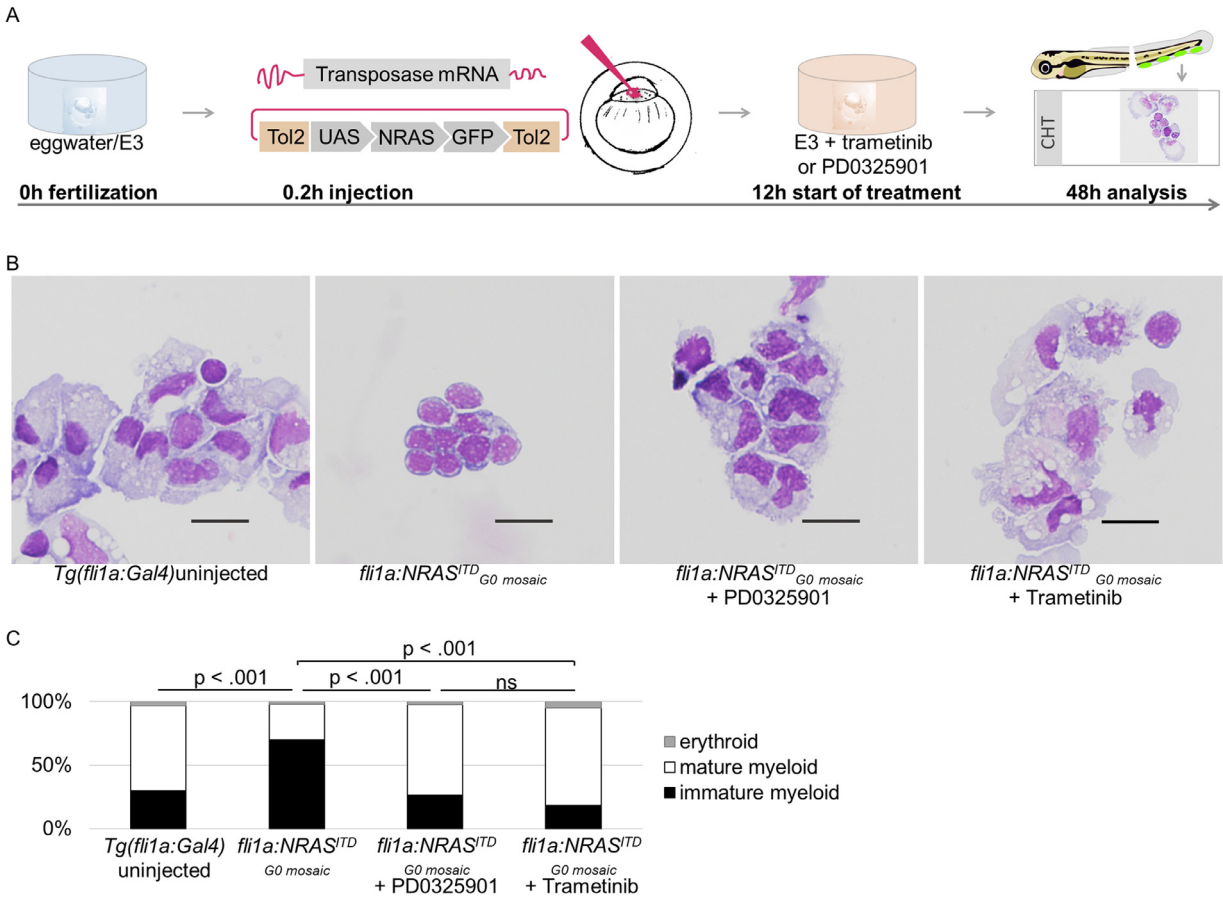


Figure 3 Targeted treatment in *NRAS*$^{ITD}$-zebrafish embryos. **(A)** The NRAS-plasmid was coinjected with Tol2 transposase messenger RNA (mRNA) into the single-cell embryo. Zebrafish embryos were incubated with trametinib or PD0325901 from 12 to 48 hours post fertilization (hpf) when analysis of the caudal hematopoietic tissue (CHT) was performed. **(B)** Images show CHT smears stained with May-Grünwald Giemsa (MGG) stain in *fli1a:NRAS*$^{ITD}{}_{G0mosaic}$ and uninjected *Tg(fli1a:Gal4)* embryos as well as trametinib- and PD0325901-treated *fli1a:NRAS*$^{ITD}{}_{G0mosaic}$ embryos. Scale bar: 10 $\mu$m. **(C)** Shown are ratios of cell populations in CHT smears from four embryos per condition as percentages. *fli1a:NRAS*$^{ITD}{}_{G0mosaic}$ embryos showed a significant increase in immature myeloid cells ($X^2$ [2, n=4] = 32.14, $p < 0.001$). After treatment of *fli1a:NRAS*$^{ITD}{}_{G0mosaic}$ embryos with PD0325901 as well as with trametinib, the cell fractions in the CHT showed no difference compared with uninjected *Tg(fli1a:Gal4)* embryos and a significant decrease in immature myeloid cells compared with *fli1a:NRAS*$^{ITD}{}_{G0mosaic}$ embryos ($X^2$ [2, n=4] = 49.78, $p < 0.001$) and ($X^2$ [2, n=4] = 74.66, $p < 0.001$) for trametinib.

Moreover, to rule out unspecific effects of plasmid injection or integration, we injected the UAS:*NRAS*$^{ITD}$-P2A-GFP plasmid in WT zebrafish embryos, thus leading to the integration of the plasmid into the DNA but preventing the expression of *NRAS*$^{ITD}$ due to the lack of activation of UAS by Gal4. In this experiment, we observed normal morphology and distribution of myeloid blood cells, ruling out the possibility that injection or plasmid integration leads to an accumulation of immature myeloid cells. Taken together, these findings support that the *NRAS*$^{ITD}$ effect does not result from unspecific plasmid integration but rather from activation of the RAS pathway.

The observed increase in immature myeloid cells in *fli1a:NRAS*$^{ITD}{}_{G0mosaic}$ embryos corresponded to the left-shifted hematopoiesis noted in the patient. A cell-autonomous effect can be assumed, as further restriction of the expression to HSPCs using the runx promoter [14] also resulted in an accumulation of immature myeloid cells. Of note, the *fli1a:NRAS*$^{wt}{}_{G0mosaic}$ embryos also showed an increase in immature myeloid cells but to a lesser extent than *fli1a:NRAS*$^{ITD}{}_{G0mosaic}$ embryos, which might be due to activation of the RAS pathway already caused by overexpression of *NRAS*$^{wt}$. However, the increase in *fli1a:NRAS*$^{ITD}{}_{G0mosaic}$ embryos was significantly higher than in *NRAS*$^{wt}$ and *NRAS*$^{G12D}$, leading to the assumption that *NRAS*$^{ITD}$ is a constitutive active variant. This is in line with data on similar insertion variants in patients with vascular anomalies described by van Eijkelenboom et al [28].

Importantly, the hematopoietic phenotype could be normalized by the MEK inhibitors PD0325901 and trametinib, suggesting that *NRAS*$^{ITD}$ acts via activation of the RAS pathway. Interestingly, this novel group of RAS ITDs seems to be rare in hematologic malignancies and may lead to MDS/MPN-U phenotypes. Further study of these rare mutations is necessary and might provide important insights into the molecular mechanism of and novel treatment options for MDS and MPD.

Unfortunately, the patient deceased before a putative treatment with a MEK inhibitor could be initiated. It will be interesting to correlate response to therapy in zebrafish to the response in patients in future projects.

In conclusion, we describe a patient with an overlapping myelodysplastic and myeloproliferative phenotype difficult to classify and an unusual duplication variant in *NRAS*. Development of a rapid zebrafish model allowed us to characterize this mutation and the effect of treatment with two MEK inhibitors. In the future, our model will allow translational researchers to assess novel variants in a clinically meaningful time frame to further improve personalized treatments in rare hematological diseases.

### Conflict of Interest Disclosure

FGK has received consulting fees from Novartis. All other authors do not have any conflicts of interest to declare in relation to this work.

### Acknowledgments

We would like to thank Dr. Christian Flotho, Dr. Ursula Kern, and Dr. Marina Mione for technical help and insightful discussion and Lauren O'Connell for drawing the zebrafish embryo schematics. This work was generated within the European Reference Network for Pediatric Cancer (PAEDCAN). It was supported by the José Carreras Leukemia-Foundation (to CCAB), the German Federal Ministry of Education and Research (BMBF) (01GM1911A and 01GM2207A "MyPred" to BS, AY, CMN, and ME), and the German Research Foundation (FOR2036, ER599/3-2 to ME). The authors acknowledge the contribution of the Center of Inborn and Acquired Blood Diseases at the Freiburg Center for Rare Diseases and the Hilda Biobank at the Department of Pediatrics and Adolescent Medicine, Freiburg, Germany.

## SUPPLEMENTARY MATERIALS

Supplementary material associated with this article can be found in the online version at https://doi.org/10.1016/j.exphem.2024.104207.

## REFERENCES

1. Arber DA, Orazi A, Hasserjian R, et al. The 2016 revision to the World Health Organization classification of myeloid neoplasms and acute leukemia. Blood 2016;127:2391–405.
2. Vardiman JW, Harris NL, Brunning RD. The World Health Organization (WHO) classification of the myeloid neoplasms. Blood 2002;100:2292–302.
3. Khoury JD, Solary E, Abla O, et al. The 5th edition of the World Health Organization classification of haematolymphoid tumours: Myeloid and histiocytic/dendritic neoplasms. Leukemia 2022;36:1703–19.
4. Emanuel PD. Myelodysplasia and myeloproliferative disorders in childhood: An update. Br J Haematol 1999;105:852–63.
5. Niemeyer CM. JMML genomics and decisions. Hematology Am Soc Hematol Educ Program 2018;2018:307–12.
6. Locatelli F, Strahm B. How I treat myelodysplastic syndromes of childhood. Blood 2018;131:1406–14.
7. Chen AT, Zon LI. Zebrafish blood stem cells. J Cell Biochem 2009;108:35–42.
8. Herwig L, Blum Y, Krudewig A, et al. Distinct cellular mechanisms of blood vessel fusion in the zebrafish embryo. Curr Biol 2011;21:1942–8.
9. Westerfield M. The Zebrafish Book: A Guide for the Laboratory Use of Zebrafish (Danio rerio). 4th Edition Eugene: University of Oregon Press; 2000.
10. Mackey AS, Redd PS, DeLaurier A, Hancock CN. Codon optimized *Tol2* transposase results in increased transient expression of a *crystallin*-GFP transgene in zebrafish. MicroPubl Biol 2020;2020. https://doi.org/10.17912/micropub.biology.000268.
11. Gibson DG, Young L, Chuang RY, Venter JC, Hutchison III CA, Smith HO. Enzymatic assembly of DNA molecules up to several hundred kilobases. Nat Methods 2009;6:343–5.
12. Kawakami K. Tol2: A versatile gene transfer vector in vertebrates. Genome Biol 2007;8(Suppl 1):S7.
13. Thompson MA, Ransom DG, Pratt SJ, et al. The cloche and spadetail genes differentially affect hematopoiesis and vasculogenesis. Dev Biol 1998;197:248–69.
14. Tamplin OJ, Durand EM, Carr LA, et al. Hematopoietic stem cell arrival triggers dynamic remodeling of the perivascular niche. Cell 2015;160:241–52.
15. Schindelin J, Arganda-Carreras I, Frise E, Kaynig V, Longair M, Pietzsch T, Preibisch S, Rueden C, Saalfeld S, Schmid B, Tinevez JY. Fiji: an open-source platform for biological-image analysis. Nat. Methods. 2012;9:676–82.
16. Cirstea IC, Kutsche K, Dvorsky R, et al. A restricted spectrum of NRAS mutations causes Noonan syndrome. Nat Genet 2010;42:27–9.
17. Altschul SF, Madden TL, Schäffer AA, et al. Gapped BLAST and PSI-BLAST: A new generation of protein database search programs. Nucleic Acids Res 1997;25:3389–402.
18. Madej T, Lanczycki CJ, Zhang D, et al. MMDB and VAST+: Tracking structural similarities between macromolecular complexes. Nucleic Acids Res 2014;42:D297–303.
19. Chen S, Francioli LC, Goodrich JK, Collins RL, Kanai M, Wang Q, Alföldi J, Watts NA, Vittal C, Gauthier LD, Poterba T. A genomic mutational constraint map using variation in 76,156 human genomes. Nature 2024;625:92–100.
20. Tate JG, Bamford S, Jubb HC, et al. COSMIC: The catalogue of somatic mutations in cancer. Nucleic Acids Res 2019;47:D941–7.
21. Piragyte I, Clapes T, Polyzou A, et al. A metabolic interplay coordinated by HLX regulates myeloid differentiation and AML through partly overlapping pathways. Nat Commun 2018;9:3090.
22. Creutzig U, van den Heuvel-Eibrink MM, Gibson B, et al. Diagnosis and management of acute myeloid leukemia in children and adolescents: Recommendations from an international expert panel. Blood 2012;120:3187–205.
23. Sebolt-Leopold JS. Advances in the development of cancer therapeutics directed against the RAS-mitogen-activated protein kinase pathway. Clin Cancer Res 2008;14:3651–6.
24. Gilmartin AG, Bleam MR, Groy A, et al. GSK1120212 (JTP-74057) is an inhibitor of MEK activity and activation with favorable pharmacokinetic properties for sustained in vivo pathway inhibition. Clin Cancer Res 2011;17:989–1000.
25. Niemeyer CM, Kratz CP. Paediatric myelodysplastic syndromes and juvenile myelomonocytic leukaemia: Molecular classification and treatment options. Br J Haematol 2008;140:610–24.
26. White Y, Bagchi A, Van Ziffle J, et al. KRAS insertion mutations are oncogenic and exhibit distinct functional properties. Nat Commun 2016;7:10647.
27. Nelson AC, Turbyville TJ, Dharmaiah S, et al. *RAS* internal tandem duplication disrupts GTPase-activating protein (GAP) binding to activate oncogenic signaling. J Biol Chem 2020;295:9335–48.
28. Eijkelenboom A, van Schaik FMA, van Es RM, et al. Functional characterisation of a novel class of in-frame insertion variants of KRAS and HRAS. Sci Rep 2019;9:8239.
29. Lalonde RL, Wells HH, Kemmler CL, et al. *pIGLET*: Safe harbor landing sites for reproducible and efficient transgenesis in zebrafish. bioRxiv 2023. 2023.12.08.570868.